AGU PUBLICATIONS

Geochemistry, Geophysics, Geosystems

TECHNICAL REPORTS: METHODS

10.1002/2015GC006009

Key Points:
- The precision of calcite quantification is compared between 2-D and conventional XRD
- The 2-D-XRD can be used for nondestructive calcite detection on thin sections or coral slabs
- The 2-D-XRD has many advantages for diagenetic screening of corals compared to conventional XRD

Supporting Information:
- Figure S1
- Figure S2
- Table S1
- Table S2

Correspondence to:
J. Smodej,
joerg.smodej@emr.rwth-aachen.de

Citation:
Smodej, J., L. Reuning, U. Wollenberg, J. Zinke, M. Pfeiffer, and P. A. Kukla (2015), Two-dimensional X-ray diffraction as a tool for the rapid, nondestructive detection of low calcite quantities in aragonitic corals, *Geochem. Geophys. Geosyst.*, *16*, 3778–3788, doi:10.1002/2015GC006009.

Received 20 JUL 2015
Accepted 27 SEP 2015
Accepted article online 26 OCT 2015
Published online 29 OCT 2015

Two-dimensional X-ray diffraction as a tool for the rapid, nondestructive detection of low calcite quantities in aragonitic corals

Jörg Smodej[1], Lars Reuning[1], Uwe Wollenberg[1], Jens Zinke[2,3,4], Miriam Pfeiffer[1], and Peter A. Kukla[1]

[1]EMR Geological Institute, RWTH Aachen, Aachen, Germany, [2]Department of Environment and Agriculture, Curtin University of Technology, Bentley, Western Australia, Australia, [3]Australian Institute of Marine Science, Nedlands, Western Australia, Australia, [4]School of Geography, Archaeology and Environmental Studies, University of the Witwatersrand, Johannesburg, South Africa

Abstract Paleoclimate reconstructions based on reef corals require precise detection of diagenetic alteration. Secondary calcite can significantly affect paleotemperature reconstructions at very low amounts of ~1%. X-ray powder diffraction is routinely used to detect diagenetic calcite in aragonitic corals. This procedure has its limitations as single powder samples might not represent the entire coral heterogeneity. A conventional and a 2-D X-ray diffractometer were calibrated with gravimetric powder standards of high and low magnesium calcite (0.3% to 25% calcite). Calcite contents <1% can be recognized with both diffractometer setups based on the peak area of the calcite [104] reflection. An advantage of 2-D-XRD over convenient 1-D-XRD methods is the nondestructive and rapid detection of calcite with relatively high spatial resolution directly on coral slabs. The calcite detection performance of the 2-D-XRD setup was tested on thin sections from fossil *Porites sp*. samples that, based on powder XRD measurements, showed <1% calcite. Quantification of calcite contents for these thin sections based on 2-D-XRD and digital image analysis showed very similar results. This enables spot measurements with diameters of ~4 mm, as well as systematic line scans along potential tracks previous to geochemical proxy sampling. In this way, areas affected by diagenetic calcite can be avoided and alternative sampling tracks can be defined. Alternatively, individual sampling positions that show dubious proxy results can later be checked for the presence of calcite. The presented calibration and quantification method can be transferred to any 2-D X-ray diffractometer.

1. Introduction

Annually banded corals provide archives for paleoclimate reconstructions at high temporal resolution. Corals from modern and fossil tropical and subtropical reefs grow millimeters to centimeters a year. During growth, their aragonite skeletons are incorporating isotopic and elemental tracers that can be used as proxies for, e.g., sea surface temperature (SST), hydrologic balance, ocean circulation, upwelling, and terrestrial runoff in seasonal resolution [*Felis and Pätzold*, 2004; *Grottoli and Eakin*, 2007]. However, a major potential cause of error within coral-based paleoclimate proxy reconstructions is diagenesis. Therefore, it is widely accepted that screening for diagenesis should be a standard procedure for modern and fossil corals [*Hendy et al*., 2007; *Allison et al*., 2007; *McGregor and Abram*, 2008]. Low magnesium calcite (LMC) occurs commonly as diagenetic phase in meteoric vadose and phreatic environments [*Longman*, 1980; *McGregor and Gagan*, 2003], but was also observed to form within microborings of living corals [*Nothdurft et al*., 2007]. High magnesium calcite (HMC) cements typically form in marine phreatic and vadose environments [*Friedman et al*., 1974]. Secondary calcite at contents as low as ~1% can already create significant artifacts in paleoclimate parameters [*McGregor and Gagan*, 2003]. X-ray diffraction (XRD) is one of the most convenient and widespread methods for the mineralogical characterization of sediment samples [*Reuning et al*., 2006; *Sepulcre et al*., 2009; *Rosleff-Soerensen et al*., 2012]. It is used routinely in combination with other techniques, such as X-radiography, SEM, and petrography, to detect diagenetic alteration in corals [*McGregor and Gagan*, 2003; *Quinn and Taylor*, 2006; *Allison et al*., 2007; *Zinke et al*., 2014]. The detection limit of calcite in a calcite-aragonite mixture can be as low as <0.2% for XRD [*Sepulcre et al*., 2009], which is crucial in selecting coral samples prior to geochemical and radiochronological analysis.

Here we evaluate the potential of a 2-D X-ray diffractometer equipped with Goebel mirrors and area detector for the rapid and nondestructive detection of calcite directly on coral slabs. Aragonite-calcite mixtures with known calcite contents in a range from 0.3% to 25% are used as powder standards for the calibration of a conventional and a 2-D-XRD setup. The detection limits and precision for both methods are evaluated statistically and compared to the literature. Subsequently, petrographic quantification of calcite cements is compared with XRD spot measure on the same thin sections to evaluate the performance of the 2-D-XRD method for low calcite contents in corals.

For coral paleoclimate reconstructions, or other similar studies using biogenic carbonates as climate archives, 2-D-XRD has great advantages, as the XRD measurements can be made directly along potential geochemical sampling transects. Diagenesis is typically patchy, especially in corals, and thus not captured by conventional XRD methods.

2. Equipment and Materials

A Bruker AXS D8 discover in $\theta-\theta$ configuration with GADDS (General Area Detector Diffraction Solution), equipped with a Copper Kα tube as X-ray source, was used as 2-D-XRD system in this study. Cross-coupled Goebel mirrors as X-ray optics lead to a parallel X-ray beam geometry, which facilitates the measurements on irregular surfaces, such as coral slabs. A pinhole collimator controls the X-ray beam size. Variable collimator pinhole diameters enable the adjustment of the radiated sample surface. Using the instrumental settings given in supporting information Table S1, a pinhole diameter of 1 mm (2 mm) results in a maximum beam size of 4.5 mm (7.9 mm) on the sample. The sample is mounted on a motorized XYZ-stage that can be ϕ-rotated during measurement. The position of each sample spot is controlled by an automated laser-video alignment system. Multiple sample points can be predefined and measured automatically. In contrast to conventional XRD systems, the area detector of the 2-D X-ray diffractometer allows the simultaneous data collection over a large 2θ and γ-angle range (Figure 1), resulting in more rapid measurements. The measured two-dimensional diffraction pattern gives better intensity and statistics for phase identification and quantitative analysis, especially for samples with texture, large grain size, or small quantity [*Sulyanov et al*., 1994]. The 2-D diffraction pattern is displayed as an image from which a 1-D profile can later be derived by integrating the measured counts over the 2-D image (Figure 1 and supporting information Table S1). For more details on the technical concept and geometric conventions of two-dimensional X-ray diffraction, see *He* [2009]. As conventional XRD system, we used a Siemens D 5000 diffractometer with knife-edge collimator, secondary graphite monochromator, scintillation counter, and a beam width of 12 mm in $\theta-2\theta$ configuration. Instrumental settings for both diffractometers are given in supporting information Table S1.

For gravimetrical powder standards, a modern coral (*Porites* sp.) and a single, inorganic, rhombohedral calcite crystal were used as a source for aragonite and low magnesium calcite (LMC), respectively. A rhodoid from the Mediterranean Sea, composed entirely of coralline red algae, was used as source for high Mg calcite (HMC). An Mg content of $\sim$18 mol % was calculated for the sample using the shift of the 104 reflection from ideal stoichiometric composition [*Lumsden and Chimahusky*, 1980]. A coralline red algae is used as standard since encrusting coralline red algae is a common source for HMC in coral skeletons [*Goffredo et al*., 2012] and a coralline algae was used as HMC standard in a benchmark publication on the calibration of conventional XRD [*Sepulcre et al*., 2009]. All samples used as standard material were cleaned in an ultrasonic bath with distilled water for 15 min and afterward dried in a drying cabinet at a temperature of 45°C to constant mass. After weighting 2 g standard material with a Sartorius microbalance (1 μg precision), they were ground to homogeneous powders for about 10 min without using liquids during preparation. All samples were measured individually to check for the purity of the standard material as monomineralogical species (supporting information Figure S1). To calibrate the two XRD systems, we manufactured 20 powder standards composed of calcite/aragonite mixtures (10 HMC and 10 LMC-standards, 0.3%–25% each, see Table 1). Aliquots of these standards were placed on cavity mount holders for XRD analysis.

Several fossil *Porites* sp. samples were recovered onshore Mauritius. The fossil coral samples were cut into slabs and their calcite content was quantified using the Siemens D 5000 powder X-ray diffractometer. Samples for which calcite was detected in quantities $<$1% were selected for thin-section preparation. The thin sections were used to quantify the content of calcite cement petrographically for areas equivalent to the X-ray beam spot size of the 2-D-XRD system using the image analysis software JMicrovision. The mineralogy

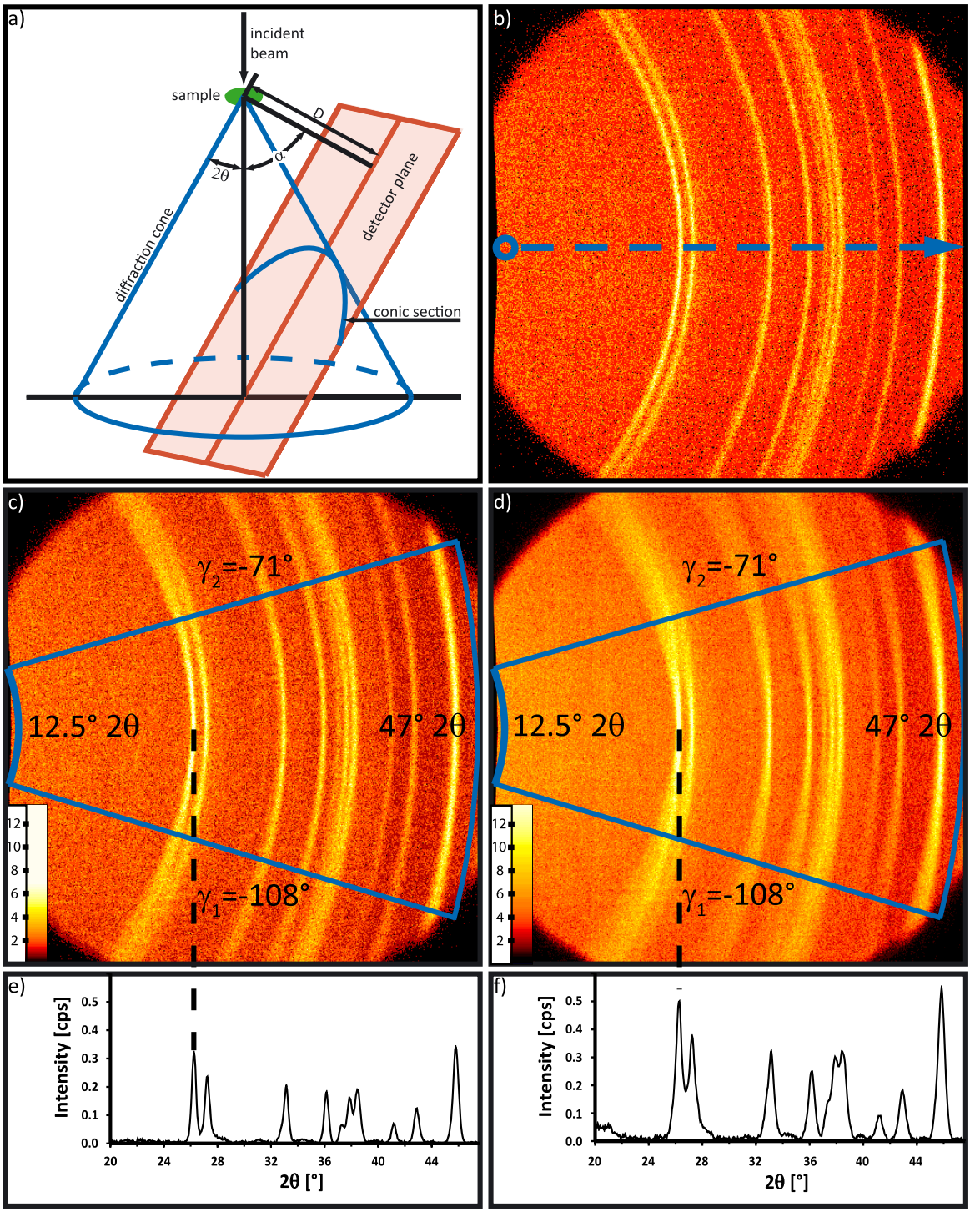

Figure 1. (a) Conic section on a 2-D detector plane resulting from the diffraction cone geometry. The plane of the 2-D detector surface intersects the diffraction cone with distance between sample and detector D, the detector swing angle ($\alpha = \theta_1 + \theta_2$) and the apex angle of the cone as twice the Bragg 2θ value (see supporting information Table S1). The conic section shape is α dependent. Diffraction frames of an aragonite powder sample and coverage comparison between (b) conventional point detector and 2-D detectors and collimator pinhole diameter of (c) 1 mm and (d) 2 mm. Scale bar is given as intensity per pixel. A conventional point detector is collecting the diffraction pattern over a range of 2θ by stepwise scanning within the diffractometer plane (along the blue arrow in Figure 1b). With a 2-D detector, the diffraction pattern can be measured simultaneously over a large 2θ and γ – angle range (area outlined in blue in Figures 1c and 1d), resulting in shorter measurement durations as well as better intensity and statistics for phase identification and quantitative analysis. Integration over this area results in a 1-D intensity versus 2θ pattern (Figures 1e and 1f), commonly known as 1-D powder diffractogram, which is used for further interpretation. The black dashed lines show the association between the aragonite [111] conic section in the 2-D-XRD diffraction frame and its peak in the corresponding 1-D diffraction pattern. In comparison to diffraction patterns from 1 mm collimator-pinhole measurements, 2 mm XRD-patterns show higher intensities but less distinct peaks due to smearing effects. Modified after *He* [2009].

Table 1. X-Ray Diffraction Calibration Results[a]

	HMC						LMC					
	ACC (%)	$\overline{AR}$	$1\sigma_m$	1σ	*R* (%)	*r*	*ACC* (%)	$\overline{AR}$	$1\sigma_m$	1σ	*R* (%)	*r*
2-D X-ray diffraction, 1 mm collimator	0.31	0.0212	0.0058	0.0076	27.15	0.0211	0.28	0.0195	0.0033	0.0043	16.84	0.0119
	0.50	0.0285	0.0081	0.0104	28.27	0.0287	0.50	0.0311	0.0027	0.0035	8.56	0.0096
	0.97	0.0542	0.0090	0.0120	16.56	0.0332	0.99	0.0743	0.0046	0.0065	6.24	0.0179
	2.02	0.0797	0.0066	0.0088	8.31	0.0243	2.04	0.1432	0.0100	0.0119	6.98	0.0331
	3.04	0.1180	0.0046	0.0053	3.90	0.0148	3.06	0.1990	0.0047	0.0057	2.37	0.0159
	5.03	0.1798	0.0017	0.0022	0.95	0.0061	5.04	0.3246	0.0099	0.0141	3.05	0.0392
	9.96	0.2974	0.0076	0.0113	2.57	0.0313	9.98	0.4691	0.0102	0.0139	2.18	0.0386
	15.01	0.3906	0.0068	0.0096	1.75	0.0265	15.00	0.6003	0.0114	0.0161	1.90	0.0448
	19.98	0.5132	0.0092	0.0120	1.80	0.0334	20.01	0.7261	0.0021	0.0028	0.29	0.0079
	24.98	0.5841	0.0063	0.0091	1.07	0.0252	25.00	0.7986	0.0098	0.0130	1.23	0.0359
2-D X-ray diffraction, 2 mm collimator	0.31	0.0132	0.0034	0.0042	25.38	0.0116	0.28	0.0187	0.0014	0.0018	7.38	0.0050
	0.50	0.0234	0.0011	0.0014	4.59	0.0038	0.50	0.0265	0.0032	0.0046	12.20	0.0128
	0.97	0.0314	0.0037	0.0051	11.65	0.0141	0.99	0.0627	0.0041	0.0060	6.53	0.0167
	2.02	0.0601	0.0054	0.0069	9.06	0.0193	2.04	0.1195	0.0062	0.0075	5.19	0.0207
	3.04	0.0911	0.0058	0.0081	6.32	0.0226	3.06	0.1791	0.0087	0.0124	4.85	0.0345
	5.03	0.1478	0.0079	0.0099	5.31	0.0274	5.04	0.2866	0.0123	0.0154	4.31	0.0427
	9.96	0.2671	0.0092	0.0120	3.46	0.0333	9.98	0.4561	0.0122	0.0161	2.67	0.0446
	15.01	0.3625	0.0040	0.0059	1.10	0.0163	15.00	0.5853	0.0140	0.0198	2.40	0.0548
	19.98	0.4942	0.0068	0.0102	1.38	0.0283	20.01	0.6926	0.0150	0.0216	2.16	0.0600
	24.98	0.5633	0.0064	0.0096	1.14	0.0266	25.00	0.8023	0.0068	0.0096	0.85	0.0267
Conventional X-ray diffraction	0.31	0.0113	0.0026	0.0042	22.78	0.0117	0.28	0.0461	0.0040	0.0049	8.66	0.0136
	0.53	0.0205	0.0017	0.0022	8.35	0.0061	0.50	0.0767	0.0141	0.0179	18.40	0.0496
	0.97	0.0406	0.0049	0.0059	12.18	0.0163	0.99	0.1107	0.0094	0.0138	8.50	0.0381
	2.02	0.0896	0.0068	0.0087	7.63	0.0242	2.04	0.1756	0.0134	0.0161	7.64	0.0446
	3.04	0.1154	0.0042	0.0060	3.62	0.0166	3.06	0.2557	0.0143	0.0209	5.59	0.0578
	5.03	0.1765	0.0054	0.0077	3.05	0.0212	5.04	0.4466	0.0566	0.0648	12.68	0.1796
	9.96	0.3226	0.0098	0.0127	3.03	0.0353	9.98	0.6814	0.0138	0.0181	2.03	0.0502
	15.01	0.4221	0.0131	0.0179	3.11	0.0495	15.03	0.7549	0.0350	0.0493	4.64	0.1365
	19.98	0.5194	0.0181	0.0254	3.48	0.0705	20.01	0.8091	0.0194	0.0267	2.39	0.0741
	24.98	0.5841	0.0140	0.0185	2.40	0.0514	24.98	0.8757	0.0100	0.0140	1.14	0.0387

[a]Calibration results include aliquot calcite contents (*ACC*), mean peak-area ratios ($\overline{AR}$), mean standard deviations ($1\sigma_m$), absolute standard deviations (1σ), repeatability (*R* (%)), and repeatability limit (*r*) for HMC-aragonite and LMC-aragonite powder standards.

of the cement seen on thin section was verified using scanning electron microscopy (SEM) in backscattered electron (BSE) mode combined with energy dispersive X-ray (EDX) analysis performed on a Zeiss SEM (FESEM SUPRA^{TM} 55; Apollo 10 SDD, EDAX).

3. Methodology

3.1. Calibration

A range of instrumental settings were tested to find the best setup for the 2-D X-ray diffraction system. The same setting was used for the thin section and powder samples. During each run, the sample stage was rotated around its *z* axis. The best separation between diffractograms of standards with ~1% calcite (LMC/HMC) and pure aragonite was achieved using the settings reported in supporting information Table S1. Using these settings, the diffraction peaks for HMC and LMC can clearly be recognized for standards containing ~1% calcite (see supporting information Figure S2).

In order to calibrate the Bruker AXS D8 (2-D-XRD) and Siemens D 5000 (conventional) diffraction systems for calcite quantification, a series of measurements was performed for powder standards with calcite contents from 0.3 to 25% (Table 1 and supporting information Table S1). A further measurement series was performed after an interval of one year for the 2-D-XRD (1 mm pinhole) as well as the conventional XRD ($n = 5$ each) using the 1% HMC standard in order to provide information on variation over time (Table 1 and supporting information Table S1). During each individual XRD run, the X-ray beam interacts only with a limited area of the sample slide and a single XRD analysis is likely not entirely representative of the true sample heterogeneity as shown by *Sepulcre et al*. [2009]. We therefore followed their recommendation to mix each sample before making a new XRD slide. The diameter of the radiated sample surface can be adjusted for the 2-D-XRD system by using different collimator pinhole diameters. D8 measurements were carried out with 1 and 2 mm collimator pinhole diameters, resulting in maximum on sample beam sizes of 4.5 and 7.9 mm, respectively.

The resulting diffractograms from both diffractometers were processed further with background subtraction utilizing Bruker AXS DIFFRAC^{plus} EVA V. 9.0 software. The background was computed and subtracted using the DIFFRAC method with a curvature value of 1 and a threshold setting of 0. Calcite content was quantified using peak-area ratios (*AR*) defined by equation (1):

$$AR = A_C/(A_C + A_A) \quad (1)$$

where A_C is the peak area of calcite [104] and A_A the peak area of aragonite [111]. Mean peak-area ratios ($\overline{AR}$), calculated from all aliquots of each powder sample, were plotted against their calcite content. Equations resulting from regression of these data points can finally be used for the quantification of calcite in unknown samples. Further, we calculated the repeatability limit r with a significance level of 95% in order to check if $\overline{AR}$ are affected by outliers [*Mullins*, 2003]. The precision of the analysis was tested as repeatability (termed reproducibility in *Sepulcre et al*. [2009]) following the definition of standard ASTM E177-14 [2014]. Repeatability *R* (%) as mean standard deviation (σ_m) in percent of the mean peak-area ratios ($\overline{AR}$) is determined as outlined in *Sepulcre et al*. [2009] using equation (2)

$$R(\%) = \sigma_m * \overline{AR}^{-1} * 100 \quad (2)$$

and compared between conventional and 2-D X-ray diffraction with 1 and 2 mm collimator pinhole diameters. ANOVA analyses (one-way, independent samples, unweighted, 95% significance level) were carried out between $\overline{AR}$ of all standards with consecutive amounts of calcite, in order to analyze the differences among their group means. In order to compare the quantification performance of the differing XRD systems, differences between variances of 2-D-XRD (1 and 2 mm pinhole) and conventional XRD were evaluated using an *F* test of equality of variance (95% significance level). The variation over time was tested using the Student's *t* test (two samples, equal variances, two-tail, 95% significance level) on peak-area ratios from the two measurement series on 2-D-XRD (1 mm pinhole) as well as conventional XRD using the 1% HMC standard.

3.2. Comparison Between Petrographic Observations and XRD Results

Thin-section analysis is an effective method for the identification of diagenetic modifications in reef corals [*McGregor and Abram*, 2008]. We used thin sections as analogues to test if the 2-D-XRD analysis is able to detect low amount of calcite directly on coral slabs. Using the image analysis software JMicrovision, the calcite content was quantified for areas equivalent to the X-ray beam spot size of the 2-D-XRD system. The mineralogy of the observed cements was further verified by scanning electron microscopy in backscattered electron (BSE) mode combined with energy dispersive X-ray (EDX) analysis as well as transmitted-light microscopy. The mineral phases aragonite and HMC of an image, resulting from the combined analyses and equivalent to the X-ray beam spot size of the 2-D-XRD system, were segmented applying threshold binarization and quantified for areas using the image analysis software JMicrovision. The calcite content, calculated from the image areas of the mineral phases, was compared to the calcite content measured by the corresponding 2-D-XRD analysis.

4. Results

4.1. Aragonite-Calcite Calibrations

Standards with calcite contents ranging from 0.3 to 25% were used for the aragonite-calcite calibration of the conventional and the 2-D X-ray diffractometer (Figures 2 and 3). For each calcite phase (LMC and HMC), the calibration of the 2-D X-ray diffractometer was performed twice, using a collimator pinhole diameter of 1 and 2 mm, respectively (Figures 2a and 3a). Second-order polynomials result in a good fit for all correlations between calcite content and peak-area ratios, except for LMC on the conventional X-ray diffractometer where a fit with a third-order polynomial is more suitable (Figure 3b). Linear equations can be used in all cases for calcite contents between 0.3% and 5% (Figures 2c–2e and 3c–3e). The mean values for the area ratios and their standard deviations for both HMC and LMC standards measured with 2-D-XRD (1 and 2 mm collimator pinhole diameter) as well as conventional XRD are reported in Table 1. ANOVA analyses show that mean area ratios in the lowest data range are not significantly different in a number of cases (HMC: 0.3 and 0.5% for conventional and 2-D-XRD with 1 mm pinhole, 0.5 and 1% for 2-D-XRD with 2 mm pinhole; LMC: 0.3 and 0.5% for 2-D-XRD with 2 mm pinhole) indicating that the quantification of such low calcite values is prone to uncertainties.

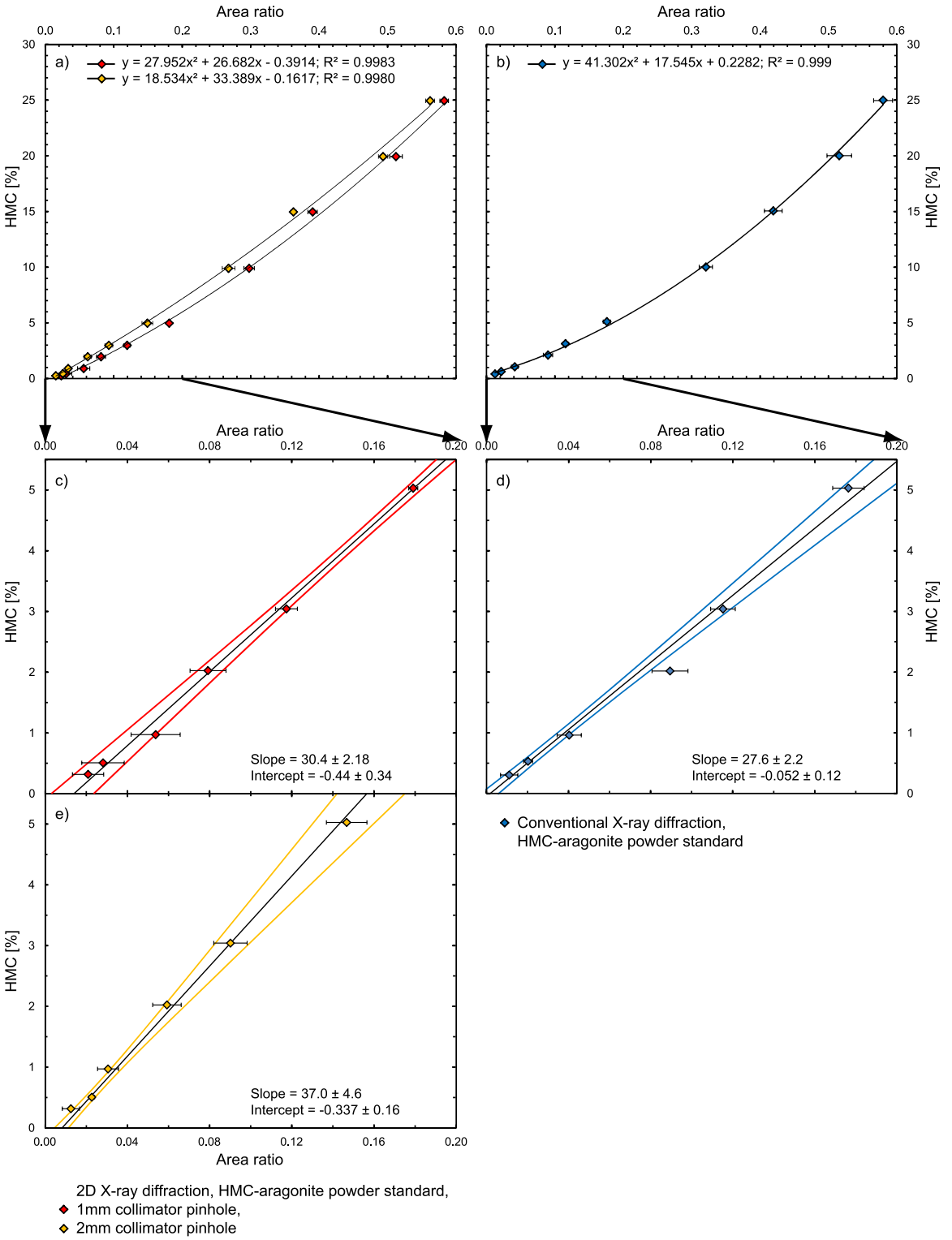

Figure 2. Correlations between HMC [104]-aragonite [111] peak-area ratio and the calcite content for 2-D X-ray diffraction with collimator pinhole-diameters of 1 mm (red diamonds) and 2 mm (yellow diamonds) and conventional X-ray diffraction (blue diamonds). Compensation curves for HMC contents from 0.3% to 25% are fitted using second-order polynomial functions as illustrated in Figures 2a and 2b. Figures 2c–2e zoom on the HMC contents of 5% and below with approximated linear correlation. Error envelopes represent the 95% confidence interval of the regression. Error bars are given at 1σ, partly hidden behind data point symbols.

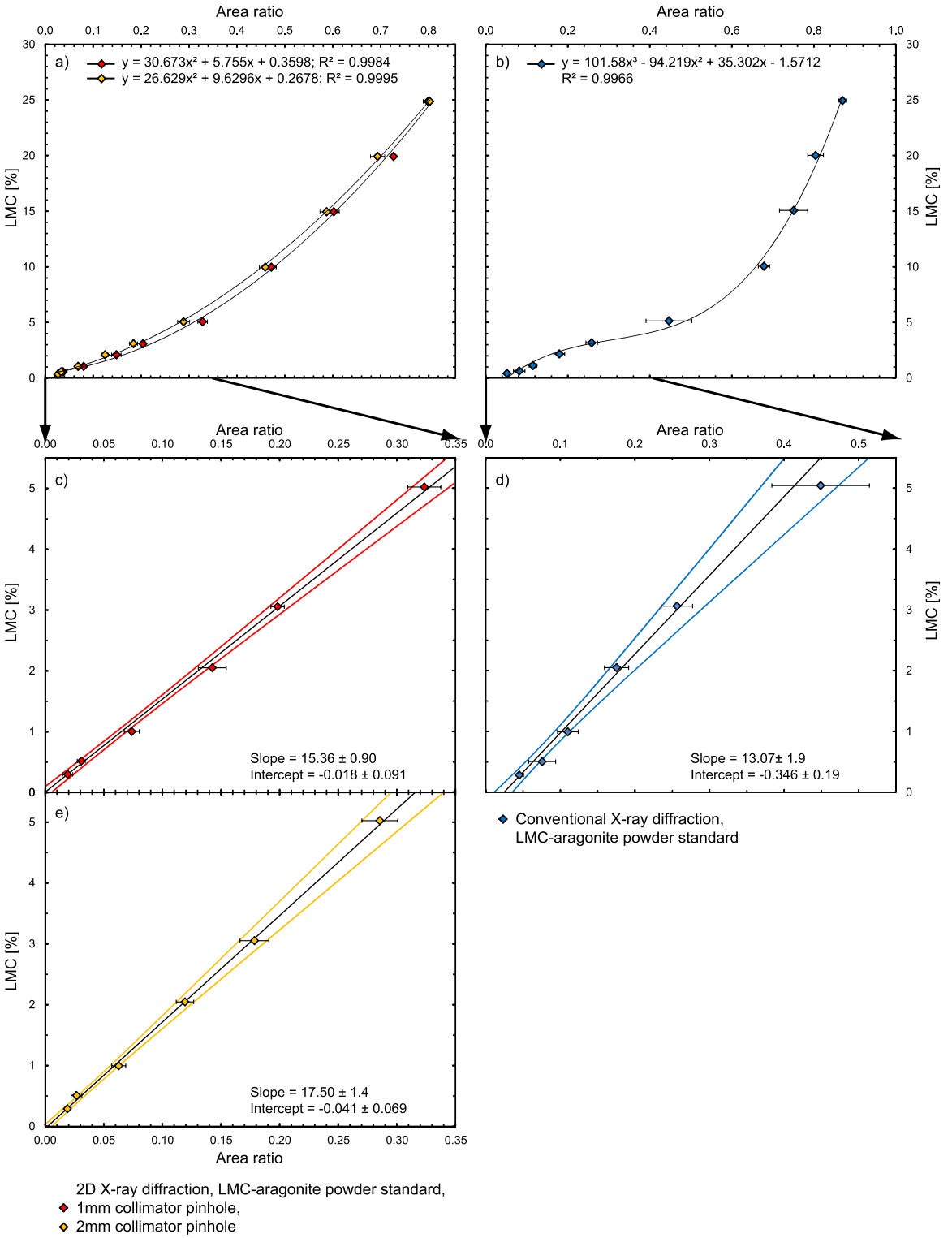

Figure 3. Correlations between LMC [104]-aragonite [111] peak-area ratio and the calcite content for 2-D X-ray diffraction and collimator pinhole-diameters 1 mm (red diamonds) and 2 mm (yellow diamonds) and 25% are fitted using (a) second-order polynomial functions for 2-D X-ray diffraction and (b) fourth order for conventional diffraction. Figures 3c–3e zoom on the LMC contents of 5% and below with approximated linear correlation. Error envelopes represent the 95% confidence interval of the regression. Error bars are given at 1σ, partly hidden behind data point symbols.

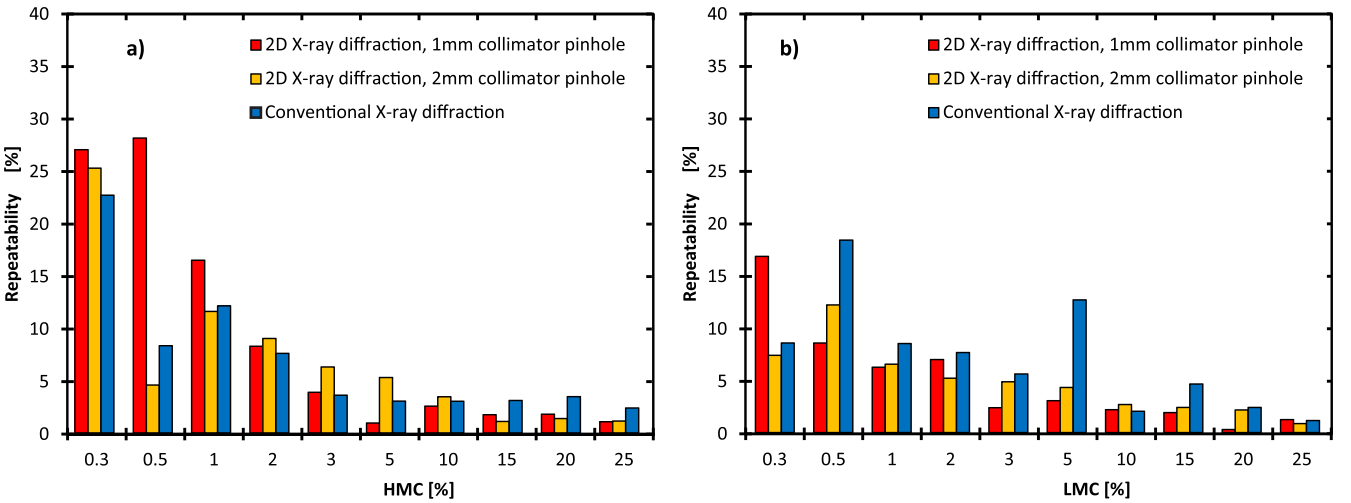

Figure 4. Comparison between the repeatability ($1\sigma_m$, $n \geq 3$) of calcite [104]-aragonite [111] peak-area ratios resulting from 2-D X-ray diffraction with collimator pinhole-diameters of 1 mm (red bars) and 2 mm (yellow bars) and conventional X-ray diffraction (blue bars). Results are presented for calibration with powder standards containing (a) HMC and (b) LMC.

The repeatability is expressed as mean standard deviation ($1\sigma_m$) in percent of the average peak-area ratios. High percentage values for the repeatability, therefore, indicate a high variability of the repeat runs of the same standard. In general, the repeatability is high for small average calcite peak-area ratios and decreases strongly with increasing ratios while absolute mean standard deviations fluctuate slightly but do not show distinct trends (Table 1).

For HMC, the repeatability varies between 0.95% and 28.27% with a mean of 7.71% for all XRD setups (Figure 4a and Table 1). Overall, the highest repeatability of the average peak-area ratios of 28.27% occurs for the 0.5% HMC standard. Using the linear equation for HMC (Figure 2c) results in a mean standard deviation of $\pm$0.39% HMC for this standard. For LMC, the precession is generally better with repeatability ranging from 0.29% to 18.40% with a mean of 5.66% for all XRD setups (Figure 4b and Table 1).

To evaluate if the observed differences in precision (Table 1 and Figure 4) between the conventional and 2-D-XRD are statistically significant, we first screened the data set (supporting information Table S1) for potential outliers exceeding the repeatability limit. The fact that only one of 432 differences between data pairs falls slightly outside the repeatability limits indicates that outliers are not significantly influencing the variability in the data set. Subsequently, we applied an *F* test for the equality of variance.

In 31 out of 40 cases, there was no significant difference between 2-D and conventional XRD. However, the measurement precision based on standard deviations is better in seven cases (5% HMC, 1 mm pinhole; 0.5, 3, 5, 20% LMC, 1 mm pinhole; 0.5, 5% LMC, 2 mm pinhole) and worse in two cases (0.5% HMC, 1 mm pinhole; 0.3% LMC, 2 mm pinhole) for 2-D-XRD compared to conventional XRD. This demonstrates that in our data set the precession for 2-D-XRD is generally similar and sometimes better than for conventional XRD.

To evaluate the longer-term stability of our calibration, we performed after one year another measurement series for the 1% HMC standard (supporting information Table S2). The Student's *t* test on peak-area ratios from the two measurement series shows that the means are not significantly different for 2-D-XRD as well as conventional XRD and therefore a significant variation over this time is not to be assumed.

4.2. Comparison Between Petrographic Observations and XRD Results

Petrographic thin-section analysis was used to test if the 2-D-XRD system is suitable for the detection of small quantities of diagenetic calcite directly on coral slaps. Thin sections were manufactured from fossil corals with very low calcite contents (<1%) measured in powder samples with conventional XRD. However, the petrographic analysis showed a patchy distribution of calcite cement in all samples, which would result in very heterogeneous calcite contents if sampled on a scale typical for geochemical analysis. Exemplarily, Figure 5 shows a thin-section segment of a diagenetically altered coral. Two different types of cement are visible (Figure 5a). Fibrous cement occurs between two coral dissepiments in the upper part of the thin-section image. Micritic, partially pelloidal cement, is concentrated between dissepiments in the center right

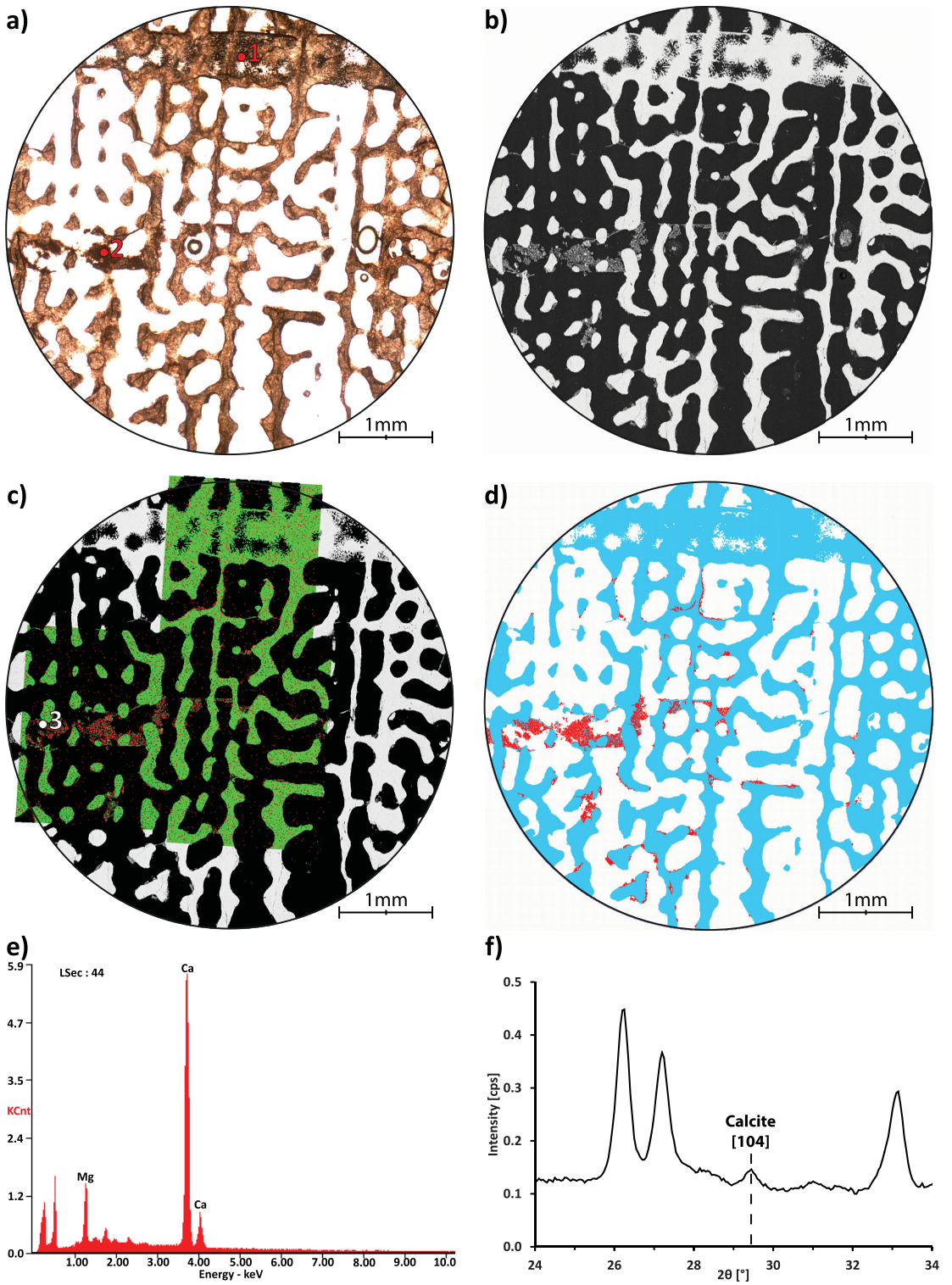

Figure 5. Thin-section analysis of a diagenetically altered coral sample. The area shown in Figures 5a–5d correlates to the X-ray beam spot size using a 1 mm pinhole diameter and a rotating sample stage. (a) Transmitted-light microscopy image of coral skeleton with (1) fibrous and (2) micritic cements. (b) BSE image: Calcite (micritic cement) shows a darker grey color compared to aragonite (fibrous cement and coral skeleton). (c) Element distribution maps for calcium (green) and magnesium (red) based on energy dispersive X-ray (EDX) analysis. High Mg counts highlight the spatial distribution of the micritic HMC cement. (d) Image analysis based on a combination of petrography, BSE, and EDX indicates HMC in red with a content of 3.5%, aragonite is shown in blue. An EDX spectrum for a spot measurements at point 3 (Figure 5c) is shown in Figure 5e and correlates with the elemental composition of HMC. Figure 5f illustrates the 1-D diffraction pattern derived from 2-D-XRD.

but is also present as thin crusts along other parts of the coral skeleton. On the BSE image (Figure 5b), the calcite mineralogy of the micritic cement is evident from its darker color compared to the coral skeleton. In contrast, the indistinguishable colors of the fibrous cement and the coral indicate that both are aragonitic. High Mg counts in the energy dispersive X-ray (EDX) measurements prove that the micritic cement consists of HMC (Figure 5f). The quantification based on image analysis of the Mg-element map, the BSE and transmitted-light microscopy (Figure 5d) results in a HMC content of 3.5%. The 2-D-XRD results for the same sample spot confirm the presence of HMC. The calcite content, calculated using the linear regression equation (Figure 2c) is 3.54 $\pm$ 0.54% (using the 95% significance envelope), indicating that the system is capable of detecting small amounts of diagenetic calcite directly on coral slabs.

5. Discussion and Summary

Conventional X-ray diffraction is routinely used to detect secondary calcite within modern and fossil corals [e.g., *Felis et al*., 2012; *Cobb et al*., 2013]. We have demonstrated that conventional and 2-D-XRD can be used to detect calcite (LMC and HMC) contents as low as 0.3%, although the quantification of HMC contents below 1% often shows uncertainties. This is consistent with a calcite detection limit of $\sim$0.2% reported in recent conventional XRD calibration studies [*Chiu et al*., 2005; *Sepulcre et al*., 2009]. It was shown statistically that the precision of the 2-D-XRD quantification in most cases is as good as or better than for the equivalent conventional XRD measurement reported in this study (Figure 4 and Table 1). A comparison to previous work on the quantification of calcite in reef corals using conventional XRD shows similar ranges for reproducibility from $\sim$1 to 25% depending on calcite contents [*Chiu et al*., 2005; *Sepulcre et al*., 2009]. Generally, 2-D-XRD and conventional XRD, therefore, seem to have comparable detection limits and a similar level of precision. However, conventional XRD has a number of shortcomings that are relevant for the use of corals (or other biogenic archives with carbonate skeletons or shells) for paleoclimatic reconstructions. The two most important ones are: (1) the method is destructive, for the preparation of conventional powder XRD samples small pieces of coral slabs are selected and ground to powder. The sampling commonly is restricted to one sample per coral or coral section. As a consequence, the XRD results are not truly representative of the sampling spots chosen for geochemical analysis. (2) Conventional XRD does not capture the small-scale distribution of diagenetic cements typical for reef corals (see e.g., Figure 5). Cement distribution is known to be very heterogeneous in modern as well as in fossil corals leading to an alternation between excellently preserved and diagenetically overprinted parts in the same coral [*McGregor and Gagan*, 2003; *Allison et al*., 2007; *Griffiths et al*., 2013]. Individual powder samples, therefore, might not represent the entire coral heterogeneity. As a result, corals that may be suitable for geochemical analysis/paleoclimatic studies may be discarded, because conventional XRD indicates the presence of calcite cements that could be avoided by locating the calcite patches along the coral slab. Or, worse still, diagenetic alteration may not be recognized since the XRD sample was taken from a pristine part of a coral. Patches of calcite diagenesis go undetected and mimic important climatic events, which are often characterized by extreme values of geochemical proxies. Especially coral d18O, which is weakly affected by calcite diagenesis [e.g., *McGregor and Gagan*, 2003], could be misinterpreted in this way. Conventional XRD made on a powder sample of the fossil coral shown in Figure 5 as thin section has a HMC content close to the detection limit of $\sim$0.2% [*Chiu et al*., 2005; *Sepulcre et al*., 2009] and could be regarded as acceptable for geochemical sampling [e.g., *Cobb et al*., 2013]. Two-dimensional XRD indicates approximately 3.5% of diagenetic calcite locally, consistent with estimates based on image analysis of the thin section (Figure 5), and it is clear that these calcite patches should be avoided for geochemical analysis. The 2-D-XRD procedure presented in our manuscript can be used to circumvent these problems since it is a nondestructive method with a relatively high spatial resolution. Thus, 2-D-XRD scanning prior to geochemical proxy sampling allows the detection of calcite and if present to define alternative sampling transects. For this application, the collimator with a pinhole diameter of 2 mm offers the coverage of a larger sample surface area and, therefore, more rapid line scans. This procedure was already successfully applied for a diagenetic screening of Holocene corals from the Seychelles that were used as paleoclimate archives [*Zinke et al*., 2014]. Alternatively, individual sample spots that show anomalies in the proxy record can be tested for secondary calcite using XRD spot measurement. This enables to differentiate between diagenesis-related artifacts and paleoclimatic events. *Nothdurft et al*. [2007] pointed out that calcite filled microborings might be undetected by XRD if they occur as a small percentage of a larger coral sample but could account for a large percentage of a given microsample. For such

problems, a collimator pinhole diameter of 1 mm may be useful, since it provides an on-sample X-ray spot size of less than 5 mm, similar to the size of diamond corers often used for sampling of, e.g., radiocarbon samples [*Fairbanks et al*., 2005].

Thus, we can summarize that the precision of the 2-D-XRD quantification is as good as or better than for the equivalent conventional XRD measurement (Figure 4 and Table 1), but with the important advantage of providing a much higher spatial resolution, so that XRD results are directly comparable to individual geochemical measurements. Under the applied setting, the shorter analysis time of the 2-D-XRD system in comparison with the conventional XRD is a further advantage (supporting information Table S1).

Other diagenetic modifications such as dissolution and aragonite cementation are not recognized by the method. XRD should, therefore, be used in combination with other techniques, such as X-radiography and SEM for a complete diagenetic screening [*Quinn and Taylor*, 2006; *Hendy et al*., 2007].

Acknowledgments
Data on all peak-area ratios of all measurements are available in supporting information Table S2. We gratefully acknowledge G. Roth for discussion and two anonymous reviewers as well as G-Cubed Editor Y. Yokoyama for their constructive comments which much improved the present manuscript. This project was funded by the DFG (PF 676/1-1 to M. Pfeiffer). The coral sample material from Mauritius was obtained during a fieldwork in 2010 with support from the Dutch NWO ALW project CLIMATCH, grant 820.01.009, and the Western Indian Ocean Marine Science Association through the Marine Science for Management program under grant MASMA/CC/2010/02. We thank the Mauritius Oceanography Institute and the ALBION Fisheries Research Centre in Mauritius for their support in fieldwork logistics and in the organization of the research and CITES permits. J.Z. was also supported by a Curtin University Senior Research Fellowship and by an Honorary Fellowship with the University of the Witwatersrand in Johannesburg, South Africa.

References

Allison, N., A. A. Finch, J. M. Webster, and D. A. Clague (2007), Palaeoenvironmental records from fossil corals: The effects of submarine diagenesis on temperature and climate estimates, *Geochim. Cosmochim. Acta*, *71*(19), 4693–4703, doi:10.1016/j.gca.2007.07.026.

ASTM E177-14 (2014), *Standard Practice for Use of the Terms Precision and Bias in ASTM Test Methods*, ASTM Int., West Conshohocken, Pa. [Available at http://www.astm.org.]

Chiu, T., R. G. Fairbanks, R. A. Mortlock, and A. L. Bloom (2005), Extending the radiocarbon calibration beyond 26,000 years before present using fossil corals, *Quart. Sci. Rev.*, *24*, 1797–1808, doi:10.1016/j.quascirev.2007.01.003.

Cobb, K. M., N. Westphal, H. Sayani, E. Di Lorenzo, H. Cheng, R. L. Edwards, and C. D. Charles (2013), Highly variable El Nino-Southern Oscillation throughout the Holocene, *Science*, *339*, 67–70, doi:10.1126/science.1228246.

Fairbanks, R. G., R. A. Mortlock, T. C. Chiu, L. Cao, A. Kaplan, T. P. Guilderson, T. W. Fairbanks, A. L. Bloom, P. M. Grootes, and M. J. Nadeau (2005), Radiocarbon calibration curve spanning 0 to 50,000 years BP based on paired Th-230/U-234/U-238 and C-14 dates on pristine corals, *Quat. Sci. Rev.*, *24*(16–17), 1781–1796, doi:10.1016/j.quascirev.2005.04.007.

Felis, T., and J. Pätzold (2004), Climate reconstructions from annually banded corals, in *Global Environmental Change in the Ocean and on Land*, edited by M. Shiyomi et al., pp. 205–227, TERRAPUB, Tokyo.

Felis, T., et al. (2012), Pronounced interannual variability in tropical South Pacific temperatures during Heinrich Stadial 1, *Nat. Commun.*, *3*, 965, doi:10.1038/ncomms1973.

Friedman, G. M., A. J. Amiel, and N. Schneide (1974), Submarine cementation in reefs—Example from Red-Sea, *J. Sediment. Petrol.*, *44*(3), 816–825.

Goffredo, S., et al. (2012), The puzzling presence of calcite in skeletons of modern solitary corals from the Mediterranean Sea, *Geochim. Cosmochim. Acta*, *85*, 187–199, doi:10.1016/j.gca.2012.02.014.

Griffiths, N., W. Muller, K. G. Johnson, and O. A. Aguilera (2013), Evaluation of the effect of diagenetic cements on element/Ca ratios in aragonitic Early Miocene (similar to 16 Ma) Caribbean corals: Implications for 'deep-time' palaeo-environmental reconstructions, *Palaeogeogr. Palaeoclimatol. Palaeoecol.*, *369*, 185–200, doi:10.1016/j.palaeo.2012.10.018.

Grottoli, A. G., and C. M. Eakin (2007), A review of modern coral DELTA O-18 and Delta C-14 proxy records, *Earth Sci. Rev.*, *81*, 67–91, doi:10.1016/j.earscirev.2006.10.001.

He, B. B. (2009), *Two-Dimensional X-ray Diffraction*, 426 pp., John Wiley, Hoboken, N. J.

Hendy, E. J., M. K. Gagan, J. M. Lough, M. McCulloch, and P. B. de Menocal (2007), Impact of skeletal dissolution and secondary aragonite on trace element and isotopic climate proxies in Porites corals, *Paleoceanography*, *22*, PA4101, doi:10.1029/2007PA001462.

Longman, M. W. (1980), Carbonate diagenetic textures from nearsurface diagenetic environments, *AAPG Bull.*, *64*, 461–487.

Lumsden, D., and J. Chimahusky (1980), Relationship between dolomite nonstoichiometry and carbonate facies parameters, in *Concepts and Models of Dolomitization*, edited by D. H. Zenger, J. B. Dunham, and R. L. Ethington, *Spec. Publ. Soc. Econ. Paleontol. Mineral.*, *28*, 123–137.

McGregor, H. V., and N. J. Abram (2008), Images of diagenetic textures in Porites corals from Papua New Guinea and Indonesia, *Geochem. Geophys. Geosyst.*, *9*, Q10013, doi:10.1029/2008GC002093.

McGregor, H. V., and M. K. Gagan (2003), Diagenesis and geochemistry of Porites corals from Papua New Guinea: Implications for paleoclimate reconstruction, *Geochim. Cosmochim. Acta*, *67*, 2147–2156, doi:10.1029/2008GC002093.

Mullins, E. (2003), *Statistics for the Quality Control Chemistry Laboratory*, 455 pp., *R. Soc. of Chem*, Cambridge.

Nothdurft, L. D., G. E. Webb, T. Bostrom, and L. Rintoul (2007), Calcite-filled borings in the most recently deposited skeleton in live-collected Porites (Scleractinia): Implications for trace element archives, *Geochim. Cosmochim. Acta*, *71*, 5423–5438, doi:10.1016/j.gca.2007.09.025.

Quinn, T. M., and F. W. Taylor (2006), SST artifacts in coral proxy records produced by early marine diagenesis in a Modern coral from Rabaul, Papua New Guinea, *Geophys. Res. Lett.*, *33*, L04601, doi:10.1029/2005GL024972.

Reuning, L., J. J. G. Reijmer, and E. Mattioli, (2006), Aragonite cycles: Diagenesis caught in the act, *Sedimentology*, *53*(4), 849–866, doi:10.1111/j.1365-3091.2006.00799.x.

Rosleff-Soerensen, B., L. Reuning, S. Back, and P. Kukla (2012), Seismic geomorphology and growth architecture of a Miocene barrier reef, Browse Basin, NW-Australia, *Mar. Pet. Geol.*, *29*(1), 233–254, doi:10.1016/j.marpetgeo.2010.11.001.

Sepulcre, S., N. Durand, and E. Bard (2009), Mineralogical determination of reef and periplatform carbonates: Calibration and implications for paleoceanography and radiochronology, *Global Planet. Change*, *66*, 1–9, doi:10.1016/j.gloplacha.2008.07.008.

Sulyanov, S. N., A. N. Popov, and D. M. Kheiker (1994), Using a 2-dimensional detector for X-ray-powder diffractometry, *J. Appl. Cryst.*, *27*, 934–942, doi:10.1107/S002188989400539X.

Zinke, J., et al. (2014), Seychelles coral record of changes in sea surface temperature bimodality in the western Indian Ocean from the Mid-Holocene to the present, *Clim. Dyn.*, *43*, 689–708, doi:10.1007/s00382-014-2082-z.